

Gradient-based Camera Exposure Control for Outdoor Mobile Platforms

Inwook Shim, Tae-Hyun Oh, Joon-Young Lee, Dong-Geol Choi, Jinwook Choi, and In So Kweon

Abstract—We introduce a novel method to automatically adjust camera exposure for image processing and computer vision applications of mobile robot platforms. Since most image processing algorithms heavily rely on low-level image features, which are largely based on local gradient information, we consider a gradient quantity to determine a proper exposure level, so that a camera is able to capture important image features robust to illumination conditions. We extend it to multi-camera system and present a new control algorithm to achieve both brightness consistency between adjacent cameras and a proper exposure level for each camera. We implement our prototype system with off-the-shelf machine vision cameras and demonstrate the effectiveness of the proposed algorithms on practical applications: pedestrian detection, visual odometry, surround-view imaging, panoramic imaging, and stereo matching.

Index Terms—Auto exposure, camera parameter control, gradient information, visual odometry, surround-view, panoramic imaging, stereo matching

I. INTRODUCTION

Recent improvements of image processing and computer vision technologies for object detection, recognition, and tracking have enabled various vision systems to operate autonomously, and this leads to the feasibility of autonomous mobile platforms. In such real-time vision-based systems, images captured from a camera are directly fed into followed algorithms as input, and the quality of images strongly affects the success of the algorithms; however, research on camera control for robust image capture has been overlooked and less studied compared to the progress of those computer vision algorithms.

Most vision systems of mobile platforms rely on a standard auto-exposure method¹ built-in the camera or a fixed exposure tuned by user handcrafting. Conventional auto-exposure methods adjust camera exposure by evaluating the average brightness of an image [1, 2, 3]. With this simple approach, one can easily find undesirably exposed images, especially

¹ I. Shim is with the Ground Autonomy Laboratory, Agency for Defense Development, 34186, Korea (e-mail: inugi00@gmail.ac.kr).

T-H. Oh is with the CSAIL, MIT, Cambridge, MA, USA (e-mail: thoh.mit.edu@gmail.com).

J-Y. Lee is with the Adobe Research, 345 Park Ave San Jose, CA 95110 (e-mail: joonyoung@live.com).

D-G. Choi is with the Robotics and Computer Vision Laboratory, Department of Electrical Engineering, KAIST, Daejeon, 305-701, Korea (e-mail: dgchoi@rcv.kaist.ac.kr).

J. Choi is with the ADAS Recognition Development Team, Hyundai Motor Group, Hwaseong-si, 445-706, Korea (e-mail: cjw0512@hyundai.com).

I.S. Kweon is with Department of Electrical Engineering, KAIST, Daejeon, 307-701, Korea (e-mail: iskweon@ee.kaist.ac.kr).

¹Specific methodologies are often not disclosed or confidential by camera manufacturers.



Fig. 1: Images are captured in different illumination conditions. From the left to the right, a camera built-in auto-exposure method, a manually tuned fixed exposure setting, and our method are used. Both the built-in auto-exposure method and the manual setting fail to capture well-exposed images for vision algorithms, while our method captures images suitable for the processing of computer vision algorithms.

when scene has a large gap between dynamic ranges of the region of interest and the background. This common phenomenon degrades the performance of followed computer vision algorithms. Overcoming the problem of diverse and challenging illumination conditions at the image capture stage is an essential prerequisite for the development of robust vision systems.

More specifically, Figure 1 shows comparisons of the standard built-in auto-exposure method and a fixed exposure setting in an outdoor environment. When the dynamic range of the scene is relatively narrow, both methods can capture well-exposed images. In this case, a single representative parameter may be easily determined by virtue of the narrow dynamic range. On the other hand, both methods provide undesirably exposed images under abruptly varying illumination conditions. The rationals behind this can be characterized as follows: 1) adaptability shortage of auto-exposure algorithm for exposure control (*i.e.*, prediction), 2) non-consideration of limited dynamic range of camera, and 3) weak criterion for assessing exposure status. We address the first and the second issues by a simulation based approach, and the third one by a gradient based metric.

In this paper, we present a new method to automatically adjust camera exposure using the gradient information. To handle severe illumination changes and a wide dynamic range of scene radiance, we simulate the proper exposure of the

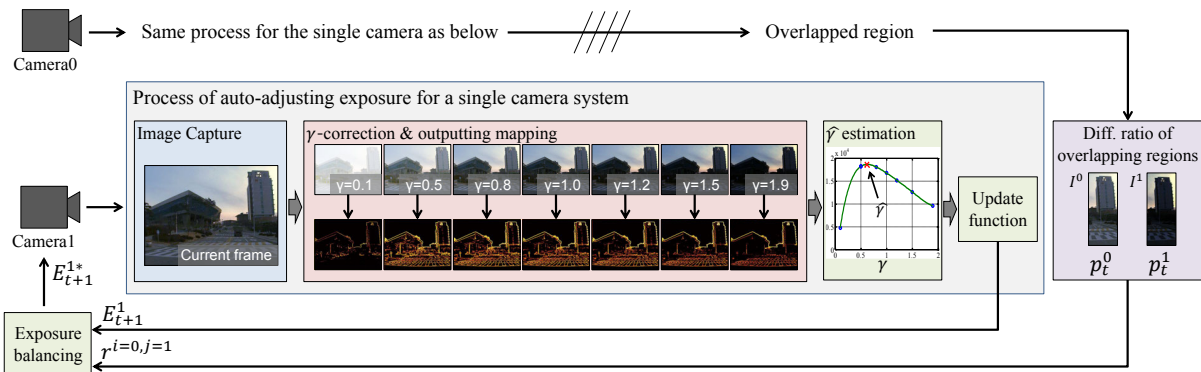


Fig. 2: The overall framework of our camera exposure control. Our method adjusts camera exposure to maximize gradient information of the captured images. We apply γ correction technique to simulate information changes by exposure variations, then update camera exposures using the real-time feedback system. In addition, we balance the exposures of multi-camera using intensity differences between neighboring cameras.

scene in the gradient domain and followed by a feedback mechanism for auto-exposure. Since the gradient domain is robust against illumination changes and has been leveraged by many computer vision algorithms, the proposed method enables to capture well-exposed images, of which enriched image features are beneficial to such computer vision algorithms.

The overall framework of our method is shown in Figure 2. To build a real-time feedback control system, we use a γ correction technique [4] that imitates exposure changes and then determines the best γ value. It implicitly guides the direction of exposure updates in the feedback system to maximize gradient information. Moreover, in the multi-camera case, our method adjusts camera exposure by taking into account neighboring cameras.

In Section II we review existing alternatives, including both direct exposure control and post-processing; however, we stress that none of these has considered the performance of followed algorithms, where enriching gradient in image may help. We then describe a gradient based criterion we developed in Section III-A, whereby a simulation based control mechanism is developed in Section III-B. A preliminary version of this paper has appeared in [5]. We extend the work by 1) improving the stability of exposure updating in Section III-C, 2) extending the proposed methodology to multi-camera system in Section IV, 3) providing further technical details of implementation, and further analyzing the behavior of the proposed method diversely in Section V. Then, we conclude this work with discussion in Section VI. Our high-level contributions can be summarized as follows:

- We propose a novel camera exposure control mechanism that leverage image gradient information to determine a proper exposure level. Specifically, we take a novel notion of simulation based exposure prediction, whereby the state of camera exposure is updated by a newly proposed control function. This shows empirically fast convergence to the target exposure level.
- We extend the approach for multi-camera setup, where exposure balancing issue across cameras arise. We pro-

pose a camera network aware exposure update method to reduce the brightness gap among neighbor cameras.

- We implement a mobile system with synchronized cameras to prove the concept of the propose methodology and to conduct fully controllable and ease experiments. We validate our method by extensive experiments with practical computer vision applications: pedestrian detection, visual odometry, surround-view imaging, panoramic imaging, and stereo matching.

II. RELATED WORK

There are several methods to control the amount of light reaching a camera sensor, namely, adjusting shutter speed, aperture size, or gain (ISO) [6]; mounting a sort of density filter [7, 8, 9]; or designing new concepts of cameras, such as computational cameras [10]. Each of them has their advantages and disadvantages. Shutter speed affects image blur, gain is related to image noise, and aperture size changes the depth of field. The other methods require external devices, such as a density filter or a new optical device. Among them, adjusting the shutter speed and gain is the most popular and desirable in vision applications for mobile platforms since it preserves a linear relationship between irradiance and intensity measurement ideally. On contrary, though the others could be good complements in some beneficial situations, they may introduce some artifacts: for example, changing aperture size or mounting a density filter² lead to changing the depth of field (spatially varying blur) or color shift respectively. These feed non-linear artifacts into subsequent vision algorithms. In this paper, we focus our review on approaches that control shutter speed and gain, and compare their criteria to determine proper parameters. We then discuss algorithmic efforts to overcome the limitation of exposure control and extensions to joint-adjustment among multiple cameras.

One conventional approach to auto-exposure is extracting the statistics of an image and controlling camera parameters to satisfy the statistics of certain conditions. The simplest way

²Specialized hardware implementation is required as in [7, 8, 9].

is measuring the average brightness over an entire image or in certain regions and adjusting it to be in the mid-range (e.g., 128 for 8-bit images) [3, 11].³ This may result in a proper exposure level for a scene where intensities are well-distributed over all regions and the dynamic range of the scene is narrow. In practice, a scene has multiple intensity distributions over an image, and this simple method may lead to under-/over-saturation of important details of an image. To overcome this limitation, there have been attempts to adopt other measures that may be robust against scene variations, such as entropy [12] and histogram [13, 14]. In this paper, we maximize the sum of log response of image gradients so that the gradient information of an image is enriched.

There are several methods that measure statistics over regions of interest (ROI) to make algorithms robust to scene variations [13, 15, 16, 17]. These methods measure the statistics of an ROI, such as the image center [11], a moving object or face regions [17], a user predefined ROI [13], or foreground regions, by separating the background [15] or back-light regions [16]. Since these methods control the camera exposure according to specific interests of an image, these are mostly preferable only for a few specific applications rather than general scenarios. Nonetheless, ROI-based methods are potentially useful to be combined and directly extended, in that other measures can be adopted in a similar framework. We also adopt the ROI approach to assess well-exposedness only over interesting regions for the surround-view imaging application as described in Section V.

Other methods exploit prior knowledge of a scene to determine the proper camera exposure. With a pre-defined reference area (black and white, brightness, or color patterns) in captured images, the exposure is adjusted according to an intensity histogram [18], color histogram [14], and image entropy [12]. While the approaches based on prior information work well in a known environment, it is hard to assume that prior information always stands in any scene, especially in most image processing applications for outdoor mobile platforms. Therefore, we focus on measuring goodness-of-fit on exposure without any reference.

To overcome the limitations of hardware and exposure control, high dynamic range (HDR) imaging provides a way to obtain well-exposed images that are both visually and physically compelling (*i.e.*, recovering irradiance). Since all the difficulties of auto-exposure come from the limited dynamic range of camera sensors, combining multi-exposure images can be an alternative, which is a typical approach of HDR [19, 20]. To maximize visual information in an HDR result, a set of images with different exposures is needed [21, 22]. However, such multi-exposure bracketing approaches are actually not suitable for dynamic scenes. Although there are HDR methods for dynamic scenes [23, 24], recovering the true irradiance of dynamic part is challenging with inputs captured at different times [25]. Even though a pair of low dynamic image with a stereo camera is simultaneously captured to generate an HDR image [26], it may still suffer from misalignment artifacts due

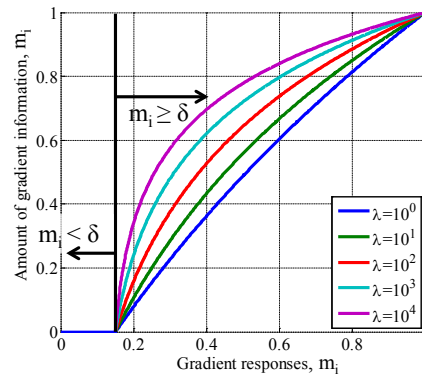


Fig. 3: Our mapping function, Eq. (1) between gradient magnitude and amount of gradient information according to the control parameters, δ and λ . We design the mapping function by reflecting general characteristics of gradient.

to imperfect stereo matching. This led to the development of a practical hardware implementation for HDR capture [7] to simultaneously capture several different exposure images for the same view. In this work, rather than an expensive specialized hardware setup, we develop a method to get well-exposed images from off-the-shelf cameras.

Up to now, previous studies have mostly relied on a single camera setup, and multi-camera exposure control has rarely been investigated. In practical image processing applications for mobile platforms, multi-camera setups are popular, and brightness similarity between cameras is required in many applications, while exposure difference between cameras is frequently observed and may be quite large due to different view points if exposure control is applied to each camera independently. Conventional multi-camera vision applications have been developed with specially designed algorithms to compensate or overcome brightness difference: correspondence matching [27], panorama imaging [28], visual odometry [29, 30], *etc.* All of these approaches are applied as post processing after image acquisition. Unavoidably, scene information beyond the dynamic range of a camera is hard to recover after an image has been captured; therefore, the working range of these post processing approaches is definitely limited by input. On the other hand, our extension to a multi-camera setup allows coherently exposed images to be obtained so that subsequent image processing algorithms get the benefits of stability and robustness.

III. GRADIENT BASED AUTOMATIC EXPOSURE CONTROL

A. Image quality from a image processing perspective

Intensity gradient is one of the most important cues for image processing and understanding. Most image features such as edges, corners, SIFT [31], and HOG [32], leverage the illumination change robustness of gradient. Moreover, the gradient information can characterize object appearance and shape well, whereby it is typically exploited in applications requiring mid-level understanding, *e.g.*, object detection, tracking, recognition, and simultaneous localization and mapping (SLAM). Therefore, capturing images with rich gradient information

³Concepts of camera metering and auto exposure are introduced in: <http://www.cambridgeincolour.com/tutorials/camera-metering.htm>.

is an important first step toward the success of many vision algorithms. In this section, we explain how the quality of exposure of a scene is evaluated in terms of gradient quantity.

In order to evaluate image quality from a machine vision perspective, it is natural to exploit the gradient domain since gradient is a dominant source of visual information for many computer vision algorithms [33]. We define well-exposed images as images having rich gradient information; therefore, we evaluate exposure by the total amount of gradient information in an image.

The gradient magnitude of a natural scene has a heavy-tailed distribution [34, 35]; therefore, most gradients have small values (including noise or zeros) relative to the maximum gradient value, and there exist sparse large gradients. Since large gradients are typically around object's boundaries, it is high probability to embed important information. On the other hand, gradients is sensitive to subtle intensity variations, *i.e.*, small magnitude gradient, image noise should be filtered properly.

To balance the importance of small and large gradients, we use a logarithm function⁴ to map the relationship between gradient magnitude and the quantity of gradient information. When we use the logarithm mapping, it may over-emphasize small gradients that occur due to image noise. For robust mapping against image noise, we modify the mapping function to discard the small noise values by simple threshold, defined as

$$\bar{m}_i = \begin{cases} \frac{1}{N} \log(\lambda(m_i - \delta) + 1) & \text{for } m_i \geq \delta \\ 0 & \text{for } m_i < \delta \end{cases} \quad (1)$$

s.t. $N = \log(\lambda(1 - \delta) + 1)$,

where m_i ⁵ is the gradient magnitude at the pixel location i , δ is the activation threshold value, λ is the control parameter to adjust mapping tendencies, and \bar{m}_i represents the amount of gradient information corresponding to gradient magnitude. Also, N is the normalization factor to bound the output range of the function to $[0, 1]$.

In Eq. (1), there are two user control parameters, δ and λ , so that these allows user to tune our method according to their needs. δ determines the activation threshold value; therefore, the mapping function regards a gradient value smaller than δ as a noise response and ignores it. λ determines the tendencies of the mapping. We can emphasize strong intensity variations by setting λ to a small value and vitalize subtle texture variations by setting λ to a large value. Figure 3 plots the mapping function according to the control parameters.

From Eq. (1), we compute the total amount of gradient information of an image as $M = \sum \bar{m}_i$. In our method, we regard the images with a larger value of M as a better exposed images that contain the rich gradient information of a scene.

B. Camera exposure auto-adjusting

Our method adjusts camera exposure at each frame such that the proposed criterion in Eq. (1) is increased. A challenge is

⁴In information theory, the quantity of information is often measured by logarithmic function, *e.g.*, entropy

⁵In this paper, the gradient magnitude is computed by Sobel operator [36], and we normalize the magnitude to the range of $[0, 1]$.

that the true relationship between exposure time and sensed gradient (or intensity) is not known [37], rather there exist complex imaging pipelines in modern cameras. Revealing such pipeline is also another challenging research area. Thus, rather than modeling the complex relationship explicitly, we propose an alternative approach that can avoid the difficulty of imaging pipeline modeling. We develop a simulation based feedback system, so that we can find a approximate direction of exposure to be updated.

We simply use a γ -mapping for exposure change simulation, whereby non-linear imaging pipelines are roughly approximated as well as under/over-saturation effects. We generate γ -mapped images $I_{out} = I_{in}^\gamma$ from a current input image I_{in} ⁶. The γ -mapping makes an image darker when $\gamma < 1$, and it makes an image brighter when $\gamma > 1$. Using this, we simulate exposure changes by a batch of γ -mapped images, compute the amount of gradient information for each image, and then find a γ such that

$$\arg \max_{\gamma} M(I_{in}^\gamma). \quad (2)$$

It is time-consuming to compute Eq. (2) from all possible γ -mapped images. For efficiency, we calculate the total amount of gradient information, M , from seven anchor images given by $\gamma \in [\frac{1}{1.9}, \frac{1}{1.5}, \frac{1}{1.2}, 1.0, 1.2, 1.5, 1.9]$, and we fit the sample values of gradient information with a fifth-order polynomial fitting. We take the maximum value of the polynomial function in the range of $\gamma = [\frac{1}{1.9}, 1.9]$ as a reference, and its corresponding γ is assigned to $\hat{\gamma}$. The parameters for Eq. (2) are empirically determined and the related experiments can be found the supplementary material⁷.

C. Camera exposure update function

In this section, we describe update rules of camera exposure given $\hat{\gamma}$. The update rules are designed such that the current exposure move toward a value that eventually leads $\hat{\gamma}$ to be 1. We propose two ways for updating camera exposure; linear update function and its extension to a nonlinear version. These two functions are designed to adjust camera exposure in inversely proportion to $\hat{\gamma}$. Figure 4 shows how the linear and nonlinear update functions work according to the control parameters, K_p and d . The details of the update functions with the control parameter are described as follows.

Linear update function. The linear update function is defined as

$$E_{t+1} = (1 + \alpha K_p (1 - \hat{\gamma})) E_t$$

$$\text{s.t. } \alpha = \begin{cases} 1/2 & \text{for } \hat{\gamma} \geq 1 \\ 1 & \text{for } \hat{\gamma} < 1, \end{cases} \quad (3)$$

where E_t is the exposure level at time t , and K_p is the proportional gain to control the convergence speed by adjusting the maximum and minimum values of the exposure update ratio. Figure 4 (a) shows the tendency of this function according to K_p . As shown in the figure, there is a trade-off between the convergence speed and stability of the update function. High K_p induces the feedback system to catch up quickly, but it may cause oscillation and overshooting.

⁶We assume that intensity is in the range of $[0, 1]$.

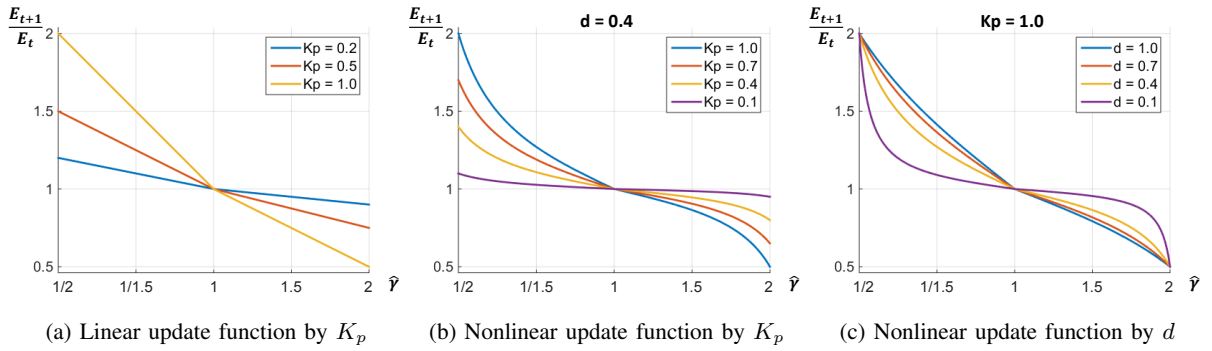


Fig. 4: Examples of linear and nonlinear update functions according to the control parameters, K_p and d .

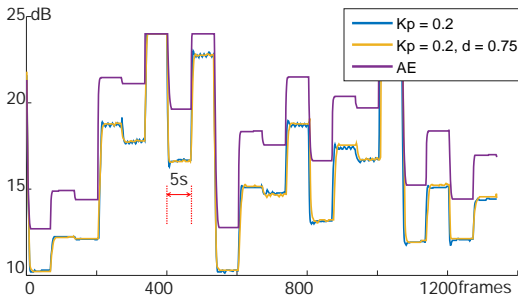


Fig. 5: Camera parameter changes according to illumination changes. The built-in auto exposure method has different exposure values from our method because of the different exposure evaluation metrics.

Nonlinear update function. The oscillation and overshooting problems of the linear update function are caused by non-smooth transition of exposure update ratios at the convergence point ($\hat{\gamma} = 1.0$) (the curved point in Figure 4 (a)). To relieve this problem, we designed a new update function, which is parametric and nonlinear. This nonlinear update function is defined as

$$\begin{aligned}
 E_{t+1} &= (1 + \alpha K_p (R - 1)) E_t \\
 \text{s.t. } R &= d \cdot \tan\{(2 - \hat{\gamma}) \cdot \arctan(\frac{1}{d}) - \arctan(\frac{1}{d})\} + 1, \\
 \alpha &= \begin{cases} 1/2 & \text{for } \hat{\gamma} \geq 1 \\ 1 & \text{for } \hat{\gamma} < 1. \end{cases}
 \end{aligned} \tag{4}$$

The R mapping is designed for realization of the shape of curves. The nonlinear update function has two control parameters K_p and d . Figure 4 (b) and (c) show how the parameters K_p and d work to control the convergence speed and stability of exposure update ratios. As with the linear update function, K_p controls the convergence speed from the current exposure level to the desired exposure level. The additional control parameter d controls the nonlinearity of the update function. As shown in the figure, smaller d makes more nonlinearity of the slope of the update ratios, which results in smooth transition at the convergence point.

To determine the proper parameter values of the linear and nonlinear update functions, we ran an experiment for parameter sweeping. For this, we control the environment as

dark room and controllable illumination due to two reasons: 1) the parameters are only related to the convergence speed and stability, thus various and continuous variation of illumination is necessary, and 2) the parameters are invariant to absolute value of illumination but only relevant to its changes, thus it is generalized to real environment.

We used five LED light sources, and each LEDs was turned on and off repeatedly with different time intervals controlled by digital timers. All the sets of parameters were tested at intervals of 0.1 values, and we empirically evaluated the convergence speed and stability of each parameter set. Figure 5 shows the results with the best performing parameters, which resulted in fast convergence with low overshoot and small oscillation. Due to the smooth slope of the nonlinear update function around the convergence point (1, 1), the nonlinear update function rarely suffered from overshoot and oscillation, while the linear update function suffered from those problems.

IV. EXPOSURE BALANCING FOR MULTI-CAMERA SYSTEM

Figure 6 shows an example of a surround-view imaging application which uses multi-camera images together. Even though images captured by each individual camera have reasonable quality, brightness inconsistency among images degrades the overall quality of the surround-view image. This kind of problems in multi-camera systems can be easily observed in many applications, such as 360° panoramic imaging and multi-camera tracking, if each camera controls its exposure individually. On the other hand, if all cameras share the same camera exposure to achieve brightness constancy, the system only captures a narrow dynamic range and may lose important information of a scene.

Based on our gradient-based exposure control development, we also address an advanced exposure control problem for a multi-camera system as it is popular in many vision systems, *e.g.*, autonomous vehicle. While independent control of each camera can capture image features better, there are many cases for multi-view image processing that favors to have consistent brightness among adjacent cameras, such as panoramic imaging and stereo matching. To take into account such cases, we present an exposure balancing algorithm that can achieve our gradient-based camera control with brightness consistency between neighboring images simultaneously.

On top of our gradient-based exposure control, we formulate an optimization problem that determines camera exposure

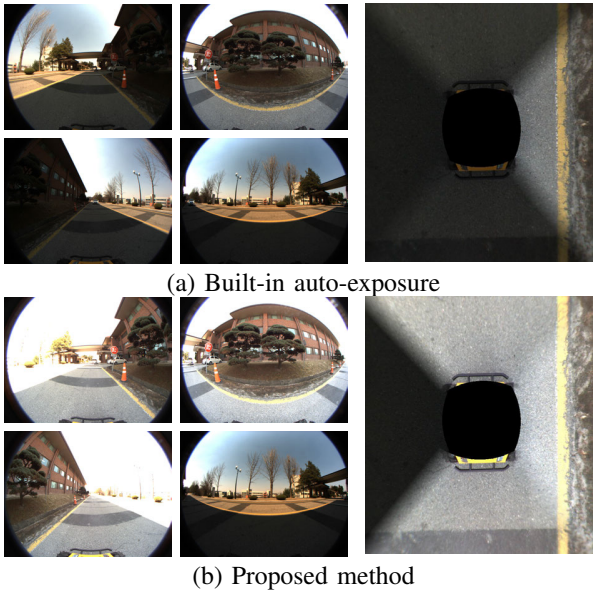


Fig. 6: The images show one of the worst case in performance of surround view application caused by low consistency between images. (a) and (b) show the original images and result of surround-view image using built-in auto-exposure and proposed method, respectively. Each camera is individually adjusted without exposure balancing.

in consideration of the balance between individual image quality and brightness constancy. Given the desired exposure of cameras obtained by Eq. (4), our optimization function considers the desired exposure as a unary term and brightness similarity in overlapped regions as a pairwise term, and it is defined as

$$\begin{aligned}
 E_{t+1}^{i*} &= \arg \min_X \alpha^i \cdot \mathcal{E}_u(i, t) + \frac{1 - \alpha^i}{N} \sum_{j \in G(i)} \mathcal{E}_p(i, j, t), \\
 \text{s.t. } \mathcal{E}_u(i, t) &= \|X - E_{t+1}^i\|^2, \\
 \mathcal{E}_p(i, j, t) &= \|X - r^{ij} \cdot E_t^{i*}\|^2, \\
 r^{ij} &= \text{median} \left(\frac{\text{mean}(p^j)}{\text{mean}(p^i) + \epsilon} \right) \quad \text{s.t. } p \in P,
 \end{aligned} \tag{5}$$

where i denotes a target camera to update the exposure level, j denotes a neighboring camera which has an overlapping region with camera i , N is the number of neighboring cameras, and t denotes the time sequence. Here, E_{t+1}^{i*} indicates an estimated optimal exposure of camera i for $t+1$ frame (next frame), E_t^{i*} is the estimated exposure value of camera i in Eq. (4), P represents a set of overlapped patches between two cameras, $\text{mean}(p)$ is the average intensity of a patch, and r^{ij} is the median value of relative brightness ratios between corresponding patches of camera i and j . We use the *median* ratio of average patches to make our solution robust to image noise and misalignment of overlapped regions.

In this optimization, $\mathcal{E}_u(\cdot)$ and $\mathcal{E}_p(\cdot)$ denote unary and pairwise terms respectively, and two terms are balanced by α . Therefore, a large α encourages more gradient information

of a scene while a small α enforces brightness similarity between cameras. Eq. (4) has a closed-form solution. For each frame, we solve Eq. (4) and Eq. (5) only one time for each camera i since it will converge through our feedback system eventually. This procedure allows for the exposure parameters to progressively adapt to a scene.

V. EXPERIMENTAL RESULTS

To validate the performance of the proposed methods, we conduct experiments on five image processing applications. We demonstrate surveillance and automotive visual odometry experiments using the proposed single camera exposure control method (Ours-single, henceforth), and also conduct experiments on surround-view, panoramic imaging, and stereo matching using the proposed multi-camera exposure control method (Ours-multi, henceforth). We compare our method to two conventional methods, a camera built-in auto-exposure (AE, henceforth) and a manually tuned fixed exposure setting (ME, henceforth). We perform all experiments with machine vision cameras which have a linear camera response function, and set up the initial exposures of the cameras by the AE method. All the results of our experiments can be found in the supplementary material⁷. All times used in this experiments refer to Korean standard time.

A. Single camera experiments

1) *Implementation*: Figure 7 shows that the camera system to evaluate the single camera exposure control. For comparative evaluation, we use three Flea3 cameras, and each camera is equipped with a Sony ICX424 CCD 1/3" sensor with a 640×480 resolution and 58.72 dB dynamic range. The three cameras are placed in parallel and are synchronized by using an internal software trigger. Each camera determines its exposure parameters by AE, ME, and Ours-single.

We use two camera parameters, *shutter speed* (exposure time) and *gain*, because controlling shutter speed affects to frame rate that is often critical according to application. We described both parameters as the exposure level E in Eq. (3). In our implementation, if we need to increase the exposure level E , first control the shutter speed according to the exposure level E until the shutter speed reached the pre-defined maximum value (we set it to 25.51ms for the following two applications, surveillance and automotive visual odometry). After the shutter speed reach the maximum value, we increase the gain. In the opposite case, the shutter speed is also adjusted when it is less than the maximum value.

2) *Surveillance application*: To validate Ours-single in a surveillance application, we recorded image sequences every two hours from 8:00 to 18:00 in a day. We collected two types of datasets.

Dataset. One dataset was collected from the three cameras after the cameras reached steady-state (SURVEILLANCE-A). Sequences were recorded for around 10 minutes for every time step. This dataset was used to compare the performance of pedestrian detection as a surveillance application, and

⁷<https://sites.google.com/site/iwshimcv/home/multicamera>



Fig. 7: Camera system for experimental validations. Three cameras has the same hardware specifications and those are synchronized by using an internal software trigger. Each camera determines exposure parameters by AE, Ours-single, and ME, respectively.

approximately 2500 pedestrians appeared in total. For the ME method, we used the same parameter in the dataset, and the parameter was initially determined at 8:00 by manual tuning.

The other dataset was taken by sweeping the full range of possible exposure levels to validate our algorithm (SURVEILLANCE-B). We sampled 210 exposure parameters that covered the full exposure range; therefore, the dataset consisted of 1260 ($= 210 \times 6$ time steps) images.

Comparison of steady-state exposures. Figure 8 shows thumbnail images of the SURVEILLANCE-B dataset. In the figure, we indicate images with rectangle markers if the image has the nearest exposure levels with one of the steady-state images of the three methods at each time step. From the thumbnails, we could easily see that the ME method suffers from illumination changes, and the AE method wipes image details out due to high luminance sky regions. On the other hand, Ours-single adjusts camera parameters to capture better exposed images with much more detail than the other methods.

Validation of our feedback system. In Figure 9, we show the progress of our feedback system, which is explained in Section III-B. To simulate extreme cases in which the illumination condition rapidly varies, we applied Ours-single to SURVEILLANCE-B. In the figure, output images of our feedback system are presented from left to right. We first put both an under-exposed image (the leftmost image on the top row) and an over-exposed image (the leftmost image on the bottom row) into our feedback system. From each image, our algorithm estimated the $\hat{\gamma}$ and updated the camera exposure according to Eq. (3). Using an updated camera exposure, we took an image that matched the exposure parameter in the dataset, and we iteratively applied our feedback system until it converged. Our system converged to the rightmost image, and it demonstrates that our method can reliably adjust camera exposure even in extreme cases. The numbers in the figure indicate $\hat{\gamma}$ estimated by Ours-single, and we can observe that $\hat{\gamma}$ converged to one as output images converged to the proper exposure level in the rightmost image.

It is also noteworthy that the scene has a much wider dynamic range than the dynamic range of our camera. In the same situation, the AE method wiped out important details in a low radiance area to prevent saturation in the sky region, as shown in Figure 10. Our method naturally adjusts camera exposure to emphasize important details by evaluating camera exposure in the gradient domain.

Pedestrian detection. We compared the performance of pedestrian detection with other exposure methods. Pedestrian detection is one of the most important tasks for surveillance. In this experiment, we performed pedestrian detection on the SURVEILLANCE-A dataset and we used a pedestrian detector in [39, 40].

Figure 10 shows example results of pedestrian detection. Images obtained by the AE method are under-exposed due to the sky region, and images obtained by the ME method are over-/under-exposed due to illumination changes. According to image quality, the pedestrian detector failed to detect humans in badly exposed images.

We use HOGgles [33] to visualize images from a perspective of image processing, so that we can qualitatively evaluate exposure control algorithm. HOGgles inverts HOG feature spaces back to a natural image; therefore, it is useful to understand how a computer sees visual images. In Figure 10, HOGgles visualizations of our method show detailed features consistently in spite of large illumination changes, while the AE and ME methods could not preserve visual information in low radiance regions due to wrong exposures. The visualization using HOGgles clearly demonstrate that our method is much more suitable than the conventional AE and ME methods for outdoor computer vision tasks.

Figure 11 shows the quantitative evaluation result of the pedestrian detection experiment. For the evaluation, the ground-truth was manually labeled for all the data. We depict the miss rate against false positives per image (FPPI) as an evaluation metric according to [41]. The evaluation metric indicates better performance as results get close to the bottom left; therefore, the figure shows that our method outperforms the other two methods.

3) *Automotive visual odometry application:* We performed visual odometry with the automotive driving dataset. Visual odometry is the process of incrementally estimating the pose of a vehicle by analyzing images captured by a camera mounted on the vehicle. It is an essential technique for autonomous navigation of vehicles and robots.

Dataset. For automotive visual odometry, we collected images taken from a vehicle driving through a campus. To validate the performance under various illumination conditions, we tried to drive almost the same path three times at 14:00, 16:00, and 18:00. We chose a path that was a closed-loop in order to easily measure the translation error between the starting point and the ending point of the path. The exposure parameter for the ME method was initialized at 14:00.

Visual odometry. For conducting visual odometry, we calibrated the camera intrinsic parameters by [42]’s method, and we also calibrated the pitch angle and height from the ground using the vanishing points of an image. We use the monocular slam algorithm in [38] for this experiment.

Figure 12 depicts the trajectories of the vehicle for a qualitative comparison. Since the vehicle drove a closed-loop path, the ground-truth of the starting points and ending points of all trajectories co-existed at (0,0) in the figure. We can observe that the results of our method have more similar trajectories among different time results and smaller distance

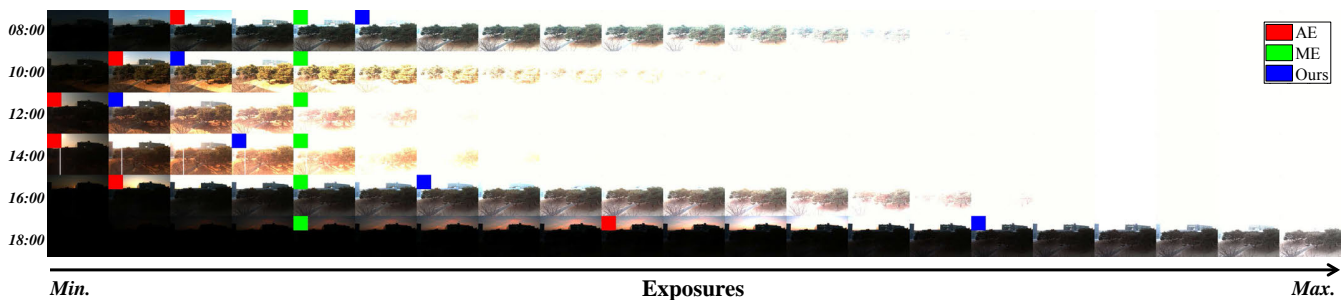


Fig. 8: Thumbnail images of the SURVEILLANCE-B dataset. Each row images are captured at every two hours from 8:00 to 18:00. In every row, we display 21 images sampled from 210 images at every time step. Images with red, green, and blue markers indicate that the images have the nearest exposure levels with steady-state exposure parameters of three methods. We recommend the readers to zoom-in to see the details clearly.

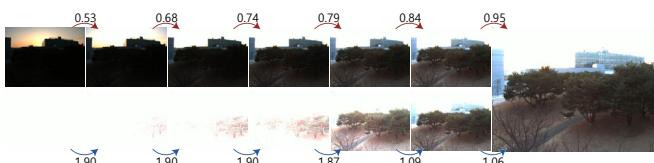


Fig. 9: Progress of our feedback system. We first put the leftmost images into our feedback system, and the system iteratively converges into the rightmost image. The numbers indicate $\hat{\gamma}$ that Ours-single estimates.

errors between the starting points and ending points than the other methods.

Images captured at two locations along the path are shown in Figure 13. In the figure, we can observe that illumination conditions varied greatly according to space and time, and both the AE and ME methods failed to successfully perform feature tracking due to under-exposure, while our method captured well-exposed images and successfully tracked image features.

In Figure 14, we present the quantitative evaluation results. The statistics of the number of inlier features are presented in (a), and the distance error ratios of each trajectory are presented in (b). Distance error ratio is computed by dividing the distance error between a starting point and an ending point of a closed-loop trajectory by the length of an estimated trajectory. Distance error ratio is used as an evaluation metric since an estimated trajectory has a scale ambiguity in monocular visual odometry. In the figure, the results of our method consistently extracted a larger number of inlier features and had smaller errors than the AE and ME methods. For robust estimation, larger number of inlier features are preferred and it is the main reason that our method shows better results than the others.

B. Multi-camera experiments

For evaluating Ours-multi, we performed experiments on three applications: surround-view imaging, panoramic imaging, stereo matching.

1) *Implementation*: Figure 15-(a) shows our multi-camera experiment system with a mobile platform, Clearpath Husky-A200. The multi-camera system has four cameras which are synchronized by a hardware trigger. The hardware trigger is set to generate synchronization signals with a frequency of

20Hz. For each camera, we used a Sony ICX445 CCD $1/3''$ sensor with a fixed focal length of $1.4mm$, so each camera had a 1288×964 resolution with a 58.44 dB dynamic range and a $185^\circ \times 144^\circ$ field-of-view (FoV). The multi-camera system was fully calibrated including both intrinsic and extrinsic parameters. To achieve the desired exposure level, we adjusted the shutter speed first until it reached the pre-defined maximum value. Then, we started adjusting the gain, same to the previous single camera experiments.

In the experiments hereafter, the maximum shutter speed was set to $49ms$, and both the shutter speed and gain parameters of each camera were adjusted by the proposed nonlinear update function Eq. (4). The exposure values among cameras were balanced by our exposure balancing method in Eq. (5). The control parameter α in Eq. (5) adjust the weights of the unary and pairwise terms. To account for varying illumination conditions well, we updated α as

$$\alpha^i = \begin{cases} (1 - R^i) + 0.5 & \text{if } R^i < 1.0, \\ R^i/2 & \text{if } R^i \geq 1.0, \end{cases} \quad (6)$$

$$\text{s.t. } R^i = \frac{E_{t+1}^i}{E_t^i} \in [0.5, 2.0],$$

where i is the camera index, and R is the exposure ratio between the current and estimated exposure values of our update function. Therefore, we give a large weight to the unary term for fast scene adaptation when the exposure levels are largely varying, while we increase the influence of the pairwise term for quick convergence to an exposure balancing point when exposure levels are stationary.

2) *Surround-view imaging application*: The surround-view imaging application is one of the most popular vision techniques in the automobile industry. A surround-view image is usually generated by stitching images from multiple cameras, and it is used to assist drivers in parking.

In this experiment, we generated a surround-view image with four partially overlapped input images as shown in Figure 16. We pre-calibrated relative poses between cameras with an assumption of flat ground, and applied a simple linear blending method [6] as a post-processing step, so that seams around view transition regions would be minimized, while the influence of post-processing would be isolated as much as possible. Figure 15-(b) depicts the fields of views (FoVs)

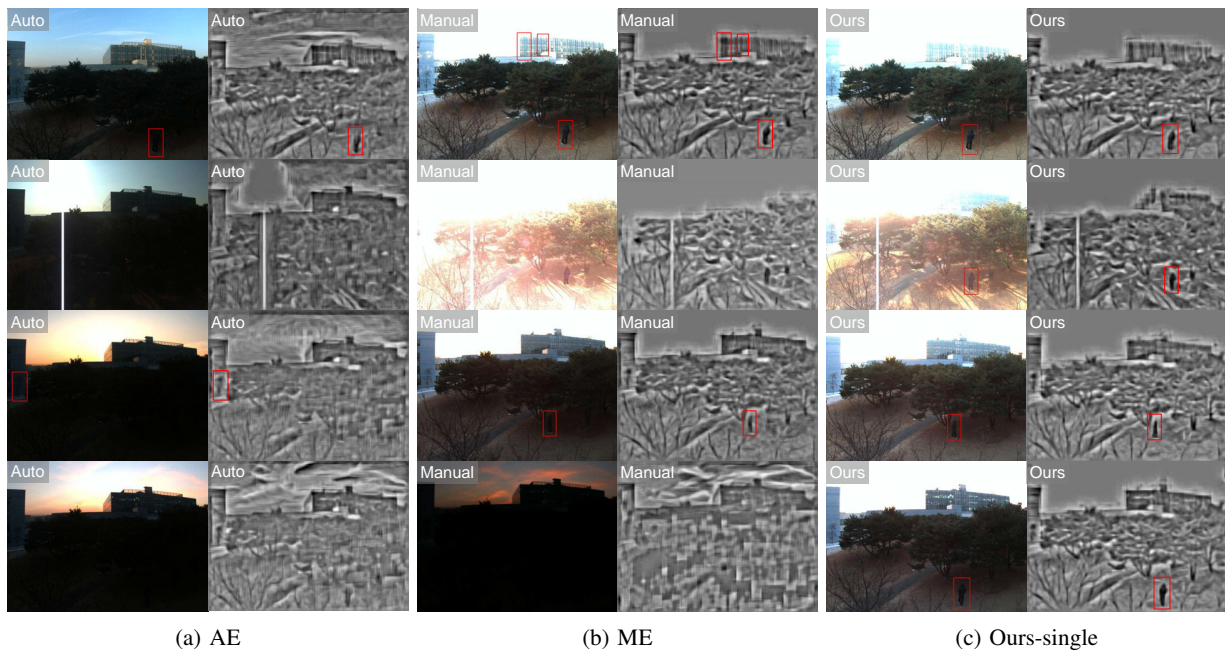


Fig. 10: The images show example results of pedestrian detection and visualizations of feature spaces using HOGgles [33]. All the input images are contained in the SURVEILLANCE-A dataset, and images in each row are captured at a same time. From the top to the bottom, images are captured around 8:00, 14:00, 16:00, and 18:00.

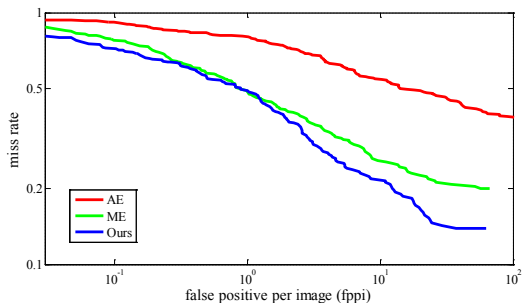


Fig. 11: Quantitative evaluation results of the pedestrian detection experiment. In the figure, it means better performance as results get closed to the bottom left.

of each camera, and (c) depicts overlapping regions between neighboring cameras from the viewpoint of a surround-view image. These overlapped regions are used to compute the relative brightness ratio r^{ij} in Eq. (5) for the exposure balancing. In this application, we are interested in the ground region of images; therefore, r^{ij} is computed only using the ground parts of input images.

Figure 16 shows the comparison result of surround-view images with different exposure control algorithms. In the figure, we show intensity changes at the boundary regions between cameras in the close-up views and also visualize the effect of exposure balancing by plotting the intensity profiles along the boundary of the rectangle (orange colored line) in the surround-view images. The colors of boundaries in the close-up views correspond to the pixel locations on the same color points in the surround-view images, respectively. As shown in

(a) and (b), the surround-view images processed by the AE and Ours-single methods have noticeably large intensity transitions at the boundary regions of two neighboring images, which is caused by the independent exposure control of each camera. In this condition, it is hard to achieve brightness constancy across all the cameras. Unlike those two methods, Ours-multi method shows relatively small intensity transitions by virtue of our exposure balancing method.

In Figure 16-(c), the un-warped images of Ours-multi are over-saturated except in the ground regions. Note that we adjust camera exposure levels only considering around the ground regions since surround-view imaging is only interested in the ground parts of the images as shown in the surround-view images.

For quantitative evaluation, we captured image sequences using a mobile robot with a multi-camera system under various illumination conditions (sunlight, cloudy, parking lot, and night scene). We drove almost the same path three times using different methods (AE, Ours-single, and Ours-multi) to obtain images for each dataset. In Figure 17, the histograms of the intensity similarity of all overlapped regions are presented. These normalized histograms were computed by the intensity ratios between images from neighboring cameras in the overlapped region for all candidates (See Figure 15 (c)). The histograms also plot an estimate of the probability density function for intensity ratio. The result obtained by Ours-multi had the smallest mean value and standard deviation of the intensity ratio, which means cameras controlled by Ours-multi take the most similar images in intensity space. This helps generate more natural surround-view images without post-processing steps, such as color transfer [43]. The movie

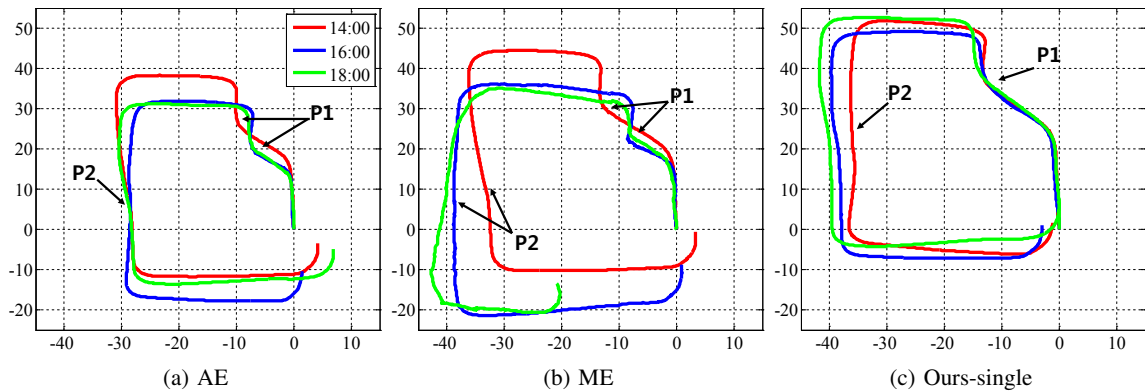


Fig. 12: Trajectories estimated by the visual odometry [38]. Since the vehicle drives a closed-loop path, the ground-truth of start points and end points of all trajectories are laid on $(0, 0)$. The results of our method have smaller estimation errors than the results of the other methods.

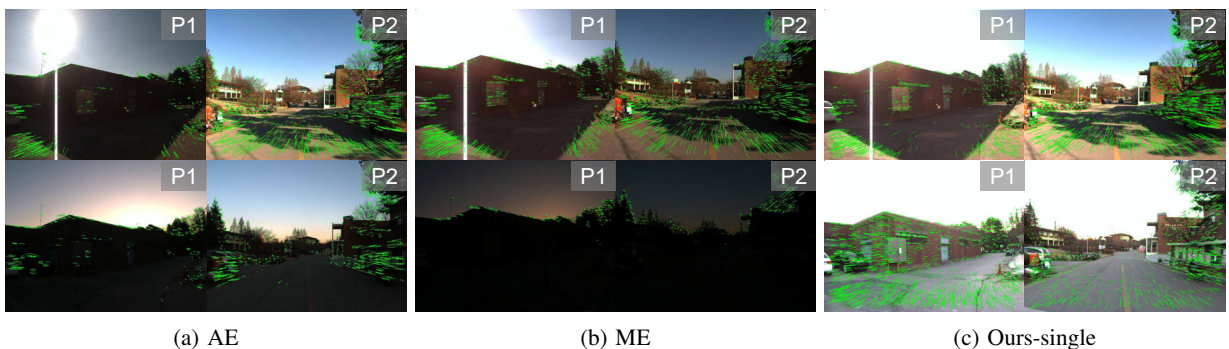


Fig. 13: Images at two locations in the path are shown. The locations are indicated in Figure 12. The top row shows images at 14:00 and the bottom row shows images at 18:00. In the images, green lines indicate tracked image features between adjacent frames.

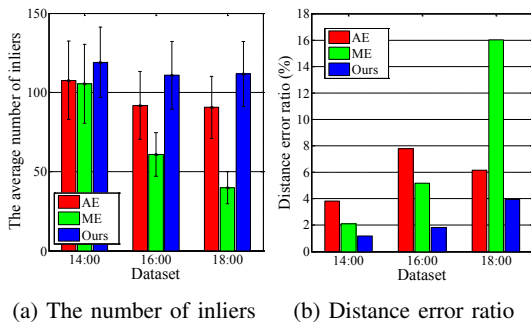


Fig. 14: Quantitative evaluation results of the visual odometry experiment. (a) mean and standard deviation of the number of inlier features, (b) relative distance errors.

clips of image sequences can be found in the supplementary material⁷.

Figure 18 shows additional qualitative comparison results of surround-view images obtained at various locations under various illumination conditions.

3) *Panoramic imaging application*: Panoramic imaging application is another good example to demonstrate the effectiveness of our method for multi-camera exposure control. This application is similar to the previous surround-view imaging application. In this application, however, we should take into account the entire region of images, so it is also important to

capture informative image features from a scene having a very wide dynamic range.

In this experiment, we used a cylindrical panorama model [44] with simple alpha and linear blending methods [6]. Additionally, for accurate matching between each pair of images, we initialized camera poses using pre-calibrated extrinsic parameters. Then, we optimized the initial camera poses by minimizing the re-projection error of matched feature points in an overlapped region of each image pair. We used the feature matching framework in [45] with the Harris corner detector [46] and BRIEF feature descriptor [47]. Then, the patches of corresponding feature points were used to compute the relative brightness ratios r^{ij} in Eq. (5).

Figure 19 shows the results of panoramic image stitching. The panoramic images with simple alpha blending clearly show differences between those produced by Ours-multi and those produced by the conventional AE method. The strong sunlight behind the building makes the dynamic range of the scene wide; therefore, the images obtained by the AE method have large brightness differences, and many informative parts of the foreground region are also under-saturated. This may lead to the failure of the following computer vision algorithms, which mainly operate for foreground objects. On the other hand, the results produced by Ours-multi show small intensity gaps in overlapped regions and also preserve important information in the foreground regions well. The linear blending

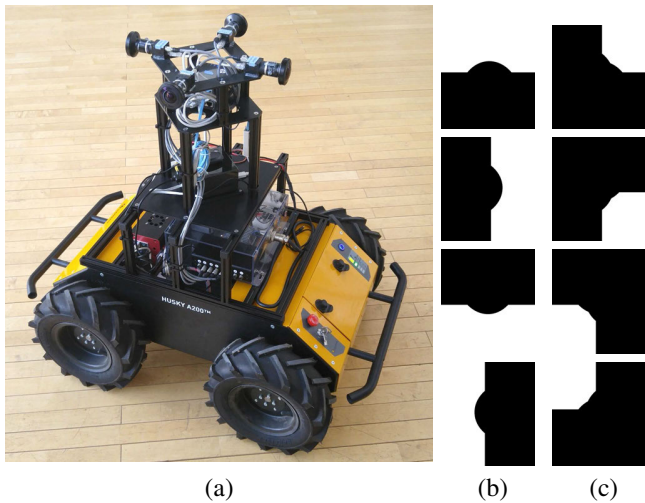


Fig. 15: (a) shows Multi-camera system with a mobile robot (Clearpath HUSKY A200). Four cameras have the same hardware specifications and those are synchronized by a hardware trigger. (b) shows valid regions for generating surround-view image. From top to bottom, the images represent FoVs for front, right, rear, and left cameras, respectively. (c) represents respective overlapping regions between neighboring cameras. For example, the top image shows overlapped FoVs between front and right cameras.

makes both results visually comfortable by smoothing the brightness difference of overlapped regions, but it could not recover information already lost in the foreground region as shown in the close-up views of (a).

4) *Stereo matching application:* In the previous two experiments, we compared differences among exposure control methods by showing the results in the color image domain. In this experiment, we applied stereo matching algorithms to verify the effectiveness of the Ours-multi method in the gradient domain. Following the panoramic imaging experiment, we used the feature matching framework in [45] and computed the relative brightness ratios r^{ij} in Eq. (5) using corresponding patches. For this experiment, we apply two representative stereo matching methods: area-correction stereo (Block, [48]) and semi-global matching (SGM, [49]).

Figure 20 shows the results of stereo matching. The block matching method computes disparity by comparing the sum of absolute differences (SAD) in a local area without any pre/post-processing and regularization. This allows us to directly compare the quality of images that affects the patch matching performance. In images obtained by the AE method, lots of visual information in the foreground regions is washed away, because of strong lighting conditions behind the foreground. In particular, regarding the pedestrian in (b) and the bush in (c), it is especially hard to recognize what/where they are in the block matching results. On the contrary, Ours-multi captures important image features in the foreground regions, so it achieves better quality of disparity maps than the AE method.

SGM improves the quality of disparity maps of both the AE

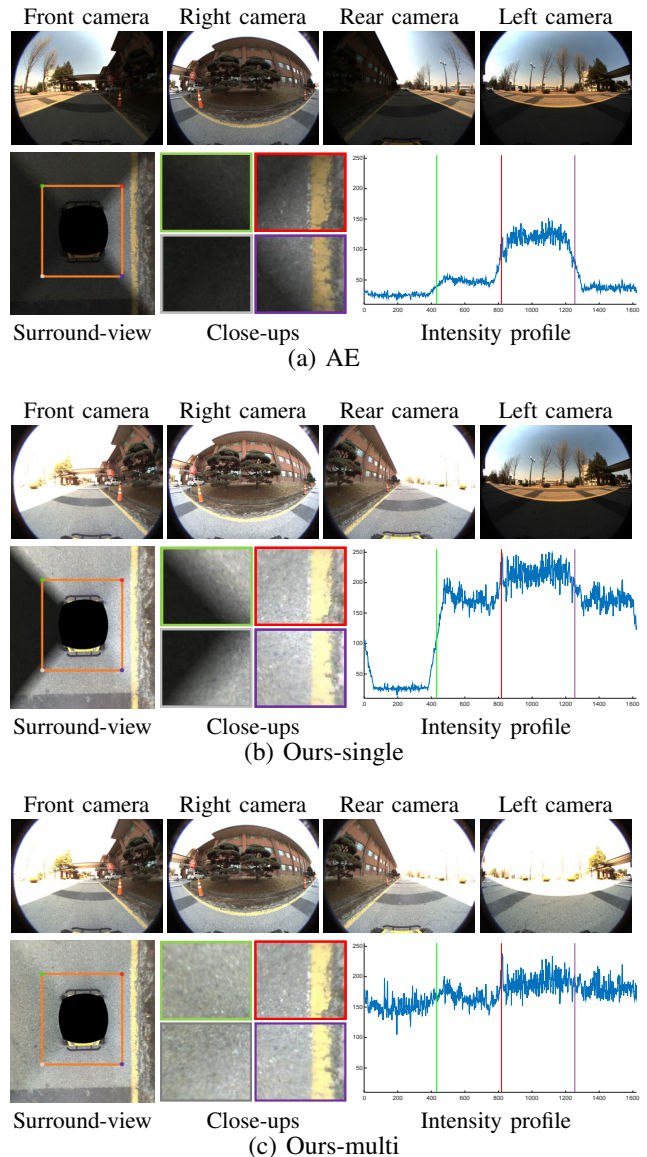


Fig. 16: Qualitative comparison of surround-view application according to exposure methods: (a) AE, (b) Ours-single, and (c) Ours-multi. The first rows of (a), (b), and (c) show the original images, and surround-view images are shown in the second rows first columns. In each second row, the image patches of second column indicate vicinity regions at green, red, purple, and gray points in the surround-view images. The last column shows 1D signals of pixel values on the orange lines of the surround-view images. We recommend readers zoom-in to see the details clearly.

and Ours-multi methods by virtue of its spatial regularization. However, there is still a visible gap between the AE and Ours-multi methods even after optimization. Ours-multi presents denser and clearer disparity maps than the AE method. This reveals the importance of image quality at the image capturing stage, which may cause difficulties that the subsequent algorithms can not deal with.

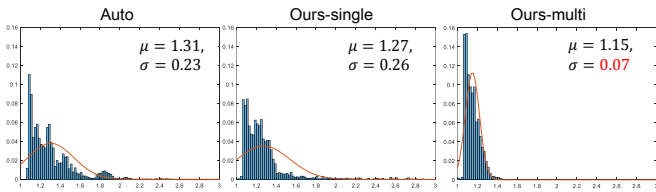


Fig. 17: Histogram of intensity ratio for all overlapped region

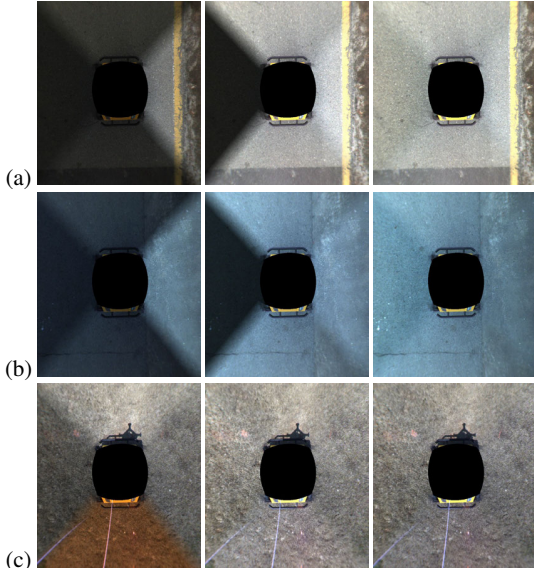


Fig. 18: Additional qualitative comparisons of surround-view imaging application at different locations.

VI. CONCLUSIONS

In this paper, we presented a novel auto-exposure method that is designed in particular for gradient-based vision systems of outdoor mobile platforms. In outdoor environments, scene radiance often has a much wider dynamic range than the possible range of cameras, and conventional camera exposure methods fail to capture well-exposed images, which results in performance degradation of subsequent computer vision-based algorithms. To solve this problem, we adjust camera exposure to maximize gradient information of a scene; therefore, our method is able to determine a proper exposure that is robust to severe illumination changes. Moreover, the exposure balancing method is also proposed for multi-camera systems.

We evaluated our methods through extensive outdoor experiments with off-the-shelf machine vision cameras using image processing and computer vision applications. We believe that our method is a good alternative/additional solution to conventional auto-exposure methods especially for outdoor computer vision systems such as surveillance monitoring system and autonomous mobile platforms.

Discussion and Limitation If a scene has mild light conditions, conventional auto-exposure methods could be a good choice to take images. Over the conventional auto-exposure methods, the proposed method is especially beneficial for capturing a scene where dark foreground regions with strong back-lighting are involved, *i.e.*, wide dynamic range.

Some images obtained by our method appear brighter than

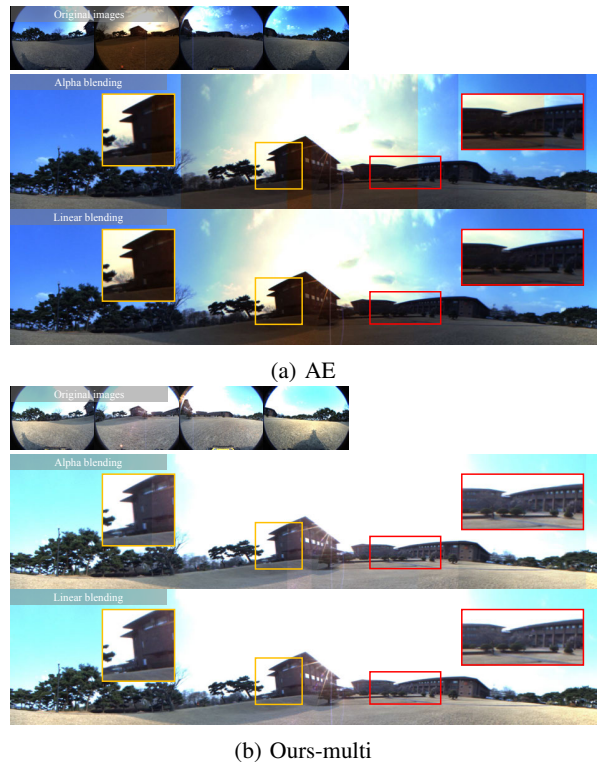


Fig. 19: Examples of panoramic images with alpha and linear blending. The top images of (a) and (b) are generated by alpha blending ($\alpha = 0.5$), and the bottom images are generated by linear blending.

the images obtained by AE in several figures. Unlike AE, which adjusts camera exposure by directly measuring brightness values, our method adjusts it for maximizing gradient information. Since gradient is invariant to offset of brightness, absolute brightness does not directly affect the propose exposure control. However, this is not an issue from the perspective of computer vision applications, as long as the dynamic range of the foregrounds is well captured or the brightness consistency between images is preserved.

In the case of multi-camera systems, a requirement of Ours-multi is that FoVs of cameras should be overlapped for matching corresponding patches in captured images. Also, our method depends on the performance of the patch matching algorithms. Therefore, we relax the sensitivity of mis-matching patches by a *median* filter as in Eq. (5). For applications where we cannot directly select the corresponding patches, *e.g.*, panoramic imaging and stereo matching, we have to consider these limitations in applying our exposure balancing method.

REFERENCES

- [1] M. Muramatsu, "Photometry device for a camera," Jan. 7 1997, uS Patent 5,592,256.
- [2] B. K. Johnson, "Photographic exposure control system and method," Jan. 3 1984, uS Patent 4,423,936.
- [3] N. Sampat, S. Venkataraman, T. Yeh, and R. L. Kremens, "System implications of implementing auto-exposure on consumer digital cameras," in *Proceedings of the SPIE Electronics Imaging Conference*, 1999, pp. 100–107.

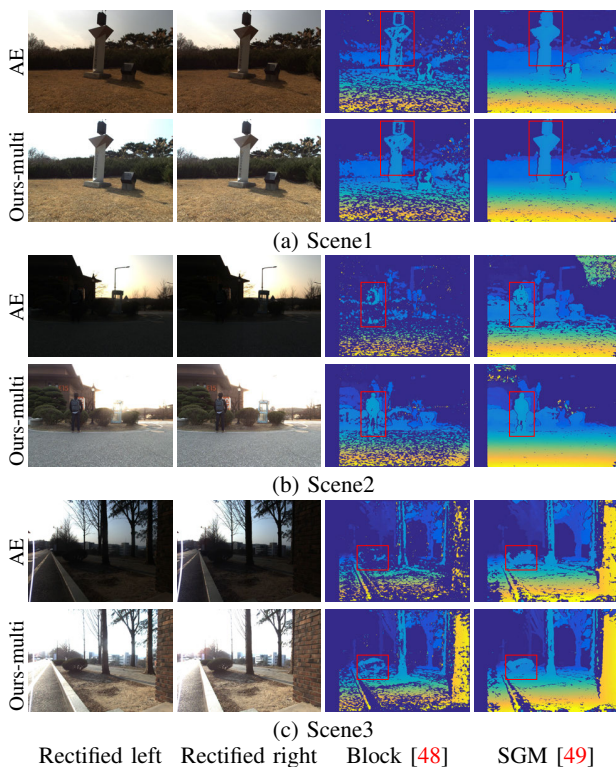


Fig. 20: Qualitative comparison of estimated disparity maps according to exposure methods: AE and Ours-multi. The images of first two columns are rectified stereo image pairs, and the third and fourth columns show the estimated disparity maps using Block [48] and SGM [49], respectively.

- [4] C. Poynton, *Digital video and HD: Algorithms and Interfaces*. Elsevier, 2012.
- [5] I. Shim, J.-Y. Lee, and I. S. Kweon, "Auto-adjusting camera exposure for outdoor robotics using gradient information," in *IEEE/RSJ International Conference on Intelligent Robots and Systems (IROS)*, 2014.
- [6] R. Szeliski, *Computer vision: algorithms and applications*. Springer Science & Business Media, 2010.
- [7] M. D. Tocci, C. Kiser, N. Tocci, and P. Sen, "A versatile hdr video production system," *ACM Transactions on Graphics (TOG)*, vol. 30, no. 4, p. 41, 2011.
- [8] M. Schoberl, A. Belz, J. Seiler, S. Foessel, and A. Kaup, "High dynamic range video by spatially non-regular optical filtering," in *IEEE International Conference on Image Processing (ICIP)*, 2012.
- [9] S. K. Nayar and T. Mitsunaga, "High dynamic range imaging: Spatially varying pixel exposures," in *IEEE Conference on Computer Vision and Pattern Recognition (CVPR)*, vol. 1, 2000, pp. 472–479.
- [10] C. Zhou and S. K. Nayar, "Computational cameras: Convergence of optics and processing," *IEEE Transactions on Image Processing (TIP)*, vol. 20, no. 12, pp. 3322–3340, 2011.
- [11] T. Kuno, H. Sugiura, and N. Matoba, "A new automatic exposure system for digital still cameras," *IEEE Transactions on Consumer Electronics*, vol. 44, no. 1, pp. 192–199, 1998.
- [12] H. Lu, H. Zhang, S. Yang, and Z. Zheng, "Camera parameters auto-adjusting technique for robust robot vision," in *IEEE International Conference on Robotics and Automation (ICRA)*, 2010, pp. 1518–1523.
- [13] N. Nourani-Vatani and J. Roberts, "Automatic camera exposure control," in *Australasian Conference on Robotics and Automation, Brisbane, Australia*, 2007.
- [14] M. Montalvo, J. M. Guerrero, J. Romeo, M. Guijarro, M. Jesús, and G. Pajares, "Acquisition of agronomic images with sufficient quality by automatic exposure time control and histogram matching," in *Advanced Concepts for Intelligent Vision Systems*, 2013, pp. 37–48.
- [15] M. Murakami and N. Honda, "An exposure control system of video cameras based on fuzzy logic using color information," in *IEEE the Fifth International Conference on Fuzzy Systems*, vol. 3, 1996, pp. 2181–2187.
- [16] J.-S. Lee, Y.-Y. Jung, B.-S. Kim, and S.-J. Ko, "An advanced video camera system with robust af, ae, and awb control," *IEEE Transactions on Consumer Electronics*, vol. 47, no. 3, pp. 694–699, 2001.
- [17] W.-C. Kao, "Real-time image fusion and adaptive exposure control for smart surveillance systems," *Electronics Letters*, vol. 43, no. 18, pp. 975–976, 2007.
- [18] A. J. Neves, B. Cunha, A. J. Pinho, and I. Pinheiro, "Autonomous configuration of parameters in robotic digital cameras," in *Pattern Recognition and Image Analysis*, 2009, pp. 80–87.
- [19] P. E. Debevec and J. Malik, "Recovering high dynamic range radiance maps from photograph," in *ACM Computer Graphics, Proceedings Annual Conference Series*, vol. 1997, 1997, pp. 369–378.
- [20] C. Lee and E. Lam, "Computationally efficient truncated nuclear norm minimization for high dynamic range imaging," *IEEE Transactions on Image Processing (TIP)*, vol. 25, no. 9, pp. 4145–4157, 2015.
- [21] S. Nuske, J. Roberts, and G. Wyeth, "Extending the dynamic range of robotic vision," in *IEEE International Conference on Robotics and Automation (ICRA)*, 2006, pp. 162–167.
- [22] N. Barakat, A. N. Hone, and T. E. Darcie, "Minimal-bracketing sets for high-dynamic-range image capture," *IEEE Transactions on Image Processing (TIP)*, vol. 17, no. 10, pp. 1864–1875, 2008.
- [23] P. Sen, N. K. Kalantari, M. Yaesoubi, S. Darabi, D. B. Goldman, and E. Shechtman, "Robust patch-based hdr reconstruction of dynamic scenes," *ACM Transactions on Graphics (SIGGRAPH Asia)*, vol. 31, no. 6, p. 203, 2012.
- [24] J. Hu, O. Gallo, K. Pulli, and X. Sun, "Hdr dehazing: How to deal with saturation?" in *IEEE Conference on Computer Vision and Pattern Recognition (CVPR)*, 2013, pp. 1163–1170.
- [25] T.-H. Oh, Y.-W. Tai, J.-C. Bazin, H. Kim, and I. S. Kweon, "Partial sum minimization of singular values in Robust PCA: Algorithm and applications," *IEEE Transactions on Pattern Analysis and Machine Intelligence (TPAMI)*, 2015.
- [26] S. Hrbar, P. Corke, and M. Bosse, "High dynamic range stereo vision for outdoor mobile robotics," in *IEEE International Conference on Robotics and Automation (ICRA)*, 2009, pp. 430–435.
- [27] Y. S. Heo, K. M. Lee, and S. U. Lee, "Robust stereo matching using adaptive normalized cross-correlation," *IEEE Transactions on Pattern Analysis and Machine Intelligence (TPAMI)*, vol. 33, no. 4, pp. 807–822, 2011.
- [28] S. J. Kim and M. Pollefeys, "Robust radiometric calibration and vignetting correction," *IEEE Transactions on Pattern Analysis and Machine Intelligence (TPAMI)*, vol. 30, no. 4, pp. 562–576, 2008.
- [29] S. J. Kim, J.-M. Frahm, and M. Pollefeys, "Joint feature tracking and radiometric calibration from auto-exposure video," in *IEEE International Conference on Computer Vision (ICCV)*, 2007.
- [30] M. Pollefeys, D. Nistér, J.-M. Frahm, A. Akbarzadeh, P. Mordohai, B. Clipp, C. Engels, D. Gallup, S.-J. Kim, P. Merrell, C. Salmi, S. N. Sinha, B. Talton, L. Wang, Q. Yang, H. Stewnius, R. Yang, G. Welch, and H. Towles, "Detailed real-time urban 3d reconstruction from video," *International Journal of Computer Vision (IJCV)*, vol. 78, no. 2-3, pp. 143–167, 2008.
- [31] D. G. Lowe, "Object recognition from local scale-invariant features," in *IEEE International Conference on Computer Vision (ICCV)*, vol. 2, 1999, pp. 1150–1157.
- [32] N. Dalal and B. Triggs, "Histograms of oriented gradients for human detection," in *IEEE Conference on Computer Vision and Pattern Recognition (CVPR)*, vol. 1, 2005, pp. 886–893.
- [33] C. Vondrick, A. Khosla, T. Malisiewicz, and A. Torralba, "HOGgles: Visualizing Object Detection Correlations," *IEEE International Conference on Computer Vision (ICCV)*, 2013.
- [34] D. Krishnan and R. Fergus, "Fast image deconvolution using hyper-laplacian priors," in *Advances in Neural Information Processing Systems (NIPS)*, 2009, pp. 1033–1041.
- [35] A. Hyvärinen, J. Hurri, and P. O. Hoyer, *Natural image statistics: a probabilistic approach to early computational vision*. Springer.
- [36] I. Sobel and G. Feldman, "A 3x3 isotropic gradient operator for image processing," a talk at the Stanford Artificial Project in, pp. 271–272, 1968.
- [37] S. J. Kim, H. T. Lin, Z. Lu, S. Susstrunk, S. Lin, and M. S. Brown, "A new in-camera imaging model for color computer vision and its application," in *IEEE Transactions on Pattern Analysis and Machine Intelligence (TPAMI)*, 2012.
- [38] A. Geiger, J. Ziegler, and C. Stiller, "Stereoscan: Dense 3d reconstruction in real-time," in *Intelligent Vehicles Symposium*, 2011.
- [39] P. Felzenszwalb, D. McAllester, and D. Ramanan, "A discriminatively trained, multiscale, deformable part model," in *IEEE Conference on*

Computer Vision and Pattern Recognition (CVPR), 2008, pp. 1–8.

- [40] P. F. Felzenszwalb, R. B. Girshick, D. McAllester, and D. Ramanan, “Object detection with discriminatively trained part-based models,” *IEEE Transactions on Pattern Analysis and Machine Intelligence (TPAMI)*, vol. 32, no. 9, pp. 1627–1645, 2010.
- [41] P. Dollár, C. Wojek, B. Schiele, and P. Perona, “Pedestrian detection: An evaluation of the state of the art,” *IEEE Transactions on Pattern Analysis and Machine Intelligence (TPAMI)*, vol. 34, no. 4, pp. 743–761, 2012.
- [42] Z. Zhang, “Flexible camera calibration by viewing a plane from unknown orientations,” in *IEEE International Conference on Computer Vision (ICCV)*, vol. 1, 1999, pp. 666–673.
- [43] J.-Y. Lee, K. Sunkavalli, Z. Lin, X. Shenand, and I. S. Kweon, “Automatic content-aware color and tone stylization,” in *IEEE Conference on Computer Vision and Pattern Recognition (CVPR)*, 2016.
- [44] R. Szeliski and H.-Y. Shum, “Creating full view panoramic image mosaics and environment maps,” in *In Proceedings of SIGGRAPH 97, Annual Conference Series*, 1997, pp. 251–258.
- [45] M. Muja and D. G. Lowe, “Fast matching of binary features,” in *IEEE International Conference on Computer and Robot Vision (CRV)*, 2012, pp. 404–410.
- [46] C. Harris and M. Stephens, “A combined corner and edge detector,” in *Alvey vision conference*, vol. 15, 1988, p. 50.
- [47] M. Calonder, V. Lepetit, C. Strecha, and P. Fua, “Brief: Binary robust independent elementary features,” *European Conference on Computer Vision (ECCV)*, pp. 778–792, 2010.
- [48] K. Konolige, “Small vision systems: Hardware and implementation,” in *Robotics Research*. Springer, 1998, pp. 203–212.
- [49] H. Hirschmüller, “Accurate and efficient stereo processing by semi-global matching and mutual information,” in *IEEE Conference on Computer Vision and Pattern Recognition (CVPR)*, vol. 2, 2005, pp. 807–814.



Inwook Shim received the B.S degree in Computer Science from Hanyang University in 2009, the M.S degree in Robotics Program from KAIST in 2011, and Ph.D degrees in Division of Future Vehicle from KAIST in 2017. He is currently a research scientist at Agency for Defense Development. He was a member of “Team KAIST” which won the first place in DARPA Robotics Challenge Finals 2015. He was a recipient of Qualcomm Innovation Award, NI finalist of NI Student Design Showcase, KAIST achievement award of Robotics, and Creativity and

Challenge award from KAIST. His research interests include image acquisition, depth processing, real-time computer vision, robot vision for autonomous system, and deep learning. He is a student member of the IEEE.



Tae-Hyun Oh is a postdoctoral associate at MIT/CSAIL. He received the BE degree (The highest ranking) in Computer Engineering from Kwang-Woon University, South Korea in 2010, and the MS and PhD degrees in Electrical Engineering from KAIST, South Korea in 2012 and 2017, respectively. He was a visiting student in the Visual Computing group, Microsoft Research, Beijing and in the Cognitive group, Microsoft Research, Redmond in 2014 and 2016, respectively. He was a recipient of Microsoft Research Asia fellowship, a gold prize of

Samsung HumanTech thesis award, Qualcomm Innovation award and a top research achievement award from KAIST. His research interests include robust computer vision and machine learning.



Joon-Young Lee received the B.S degree in Electrical and Electronic Engineering from Yonsei University, Korea in 2008. He received the M.S and Ph.D degrees in Electrical Engineering from KAIST, Korea in 2009 and 2015, respectively. He is currently a research scientist at Adobe Research. His research interests include deep learning, photometric image analysis, image enhancement, and computational photography. He is a member of the IEEE.



Dong-Geol Choi received the B.S and M.S degree in Electric Engineering and Computer Science from Hanyang University in 2005 and 2007, respectively, and the Ph.D degrees in the Robotics Program from KAIST in 2016. He is currently a post-doctoral researcher at the Information & Electronics Research Institute, in KAIST. His research interests include sensor fusion, autonomous robotics, and artificial intelligence issues. Dr.Choi received a fellowship award from Qualcomm Korea R&D Center in 2013. He was a member of “Team KAIST,” which won the

first place in DARPA Robotics Challenge Finals 2015.



Jinwook Choi Jinwook Choi (S09) received the B.S. and Ph.D. degrees from the School of Electrical and Electronic Engineering, Yonsei University, Seoul, Korea, in 2008 and 2014, respectively. He is currently a Senior Research Engineer with the ADAS Development Team of Automotive Research and Development Division, Hyundai Motor Company, Korea. His research interests include 2D/3D image and video processing, computer vision, hybrid sensor systems, and intelligent vehicle systems.



In So Kweon received the B.S. and M.S. degrees in Mechanical Design and Production Engineering from Seoul National University, Seoul, Korea, in 1981 and 1983, respectively, and the Ph.D. degree in Robotics from the Robotics Institute, Carnegie Mellon University, Pittsburgh, Pennsylvania, in 1990. He worked for the Toshiba R&D Center, Japan, and joined the Department of Automation and Design Engineering, KAIST, Seoul, Korea, in 1992, where he is now a professor with the Department of Electrical Engineering. His research interests are sensor

fusion, color modeling and analysis, visual tracking, and visual SLAM. He was the general chair for the Asian Conference on Computer Vision 2012 and he is on the honorary board of the International Journal of Computer Vision (IJCV). He has been serving as a director for the Personal Plug and Play DigiCar Center which is one of the National Core Research Center since 2010. He was a member of Team KAIST which won the first place in DARPA Robotics Challenge Finals 2015.